Robust Control Analysis Of A Gas-Turbine Aeroengine

Aznan Ezraie Ariffin and Neil Munro, *Fellow, IEEE*

***Abstract*—In this paper, an application of recent robust stability analysis tools for uncertain systems is presented. It is shown that these analysis techniques can provide an alternative method to the now well-established H^∞ approach, in providing a simpler analytical insight into the problem in hand. A study of part of the control system for the Rolls-Royce Pegasus aeroengine at various operating conditions is presented, and it is shown how these tools can assist in improving the robust stability and performance of the engine.**

***Index Terms*—Aircraft engine control, robust parametric approach.**

I. Introduction

THE $\boldsymbol{H}^\infty$ approach to robust control system design [5] is now well established. This essentially considers the effects of additive $[G(s)+\Delta(s)]$ or multiplicative $[G(s)[1+\Delta(s)]]$ unstructured perturbations, $\Delta(s)$, of the nominal system transfer-function matrix, $G(s)$, with $\boldsymbol{H}^\infty$-norm bounds on the perturbation $\Delta(s)$. This can also be combined with structured singular-valued (μ) synthesis for structured uncertainties [10]. An alternative approach, which takes into account the structure of the perturbations by assuming that some parameters (usually physical parameters) are known to lie within certain bounds or tolerances, has emerged more recently [3]. This results in a polytope formulation, which corresponds to the rank one case for μ.

The focus of this paper is on the second approach, for the following reasons [9].

1) Parameter bounds usually can be obtained from physical considerations, while it is often difficult to define meaningful bounds on $\Delta(s)$.
2) Models of perturbations in the frequency-domain that have proved successful (e.g., gain or phase perturbations) cannot represent parameter perturbation as a special case.
3) In many practical cases, after deriving an appropriate uncertainty model in the parameter space, the resulting uncertainty in the frequency-response model is negligible; i.e., it perturbs the Nyquist plot in a small neighborhood of the origin.
4) The classical gain and phase margin model becomes a special case of a more general uncertainty model in the space of transfer-function coefficients, after introducing an uncertain complex gain coefficient.

This paper is devoted to the consideration of a real system in the form of an aeroengine and its locally linearized models, and to the discussion of certain uncertainties, which arise mainly due to manufacturing tolerances. This aircraft gas-turbine engine control system design study will provide an example of the application of some recent robust control system analysis techniques, as described by Barmish and Tempo [4] and Fu [6]. In this investigation, a single-input/single-output (SISO) control system is considered, with considerable attention being attached to the ability to assign uncertainty to the components of the fuel-system subassembly. Hence, the thrust of this paper is on the application of systematic methods for robust stability analysis.

II. Problem Formulation

A. Preliminaries

The turbofan engine model to be considered in this study is a model of the Rolls-Royce Pegasus vectored-thrust turbofan engine, together with its fuel-servo and a typical engine-controller [11]. The layout of the engine is shown in Fig. 1, where P_1 and T_1 are the engine intake pressure and temperature, F is the fuel flow, N_H and N_L are the high-pressure and low-pressure compressor spool speeds, P_3 and P_2 are the high-pressure and low-pressure compressor delivery pressures, T_j is the jet-pipe temperature, T_3 is the high-pressure compressor delivery temperature, and XGF and XGR are the front and rear nozzle thrusts, respectively. A schematic diagram of the Pegasus engine fan-speed governor control scheme is depicted in Fig. 2, and a previous design for the fan-speed governor, and all the necessary data, are presented in Appendix B.

The main source of uncertainty to be considered is imparted by specified limits on the fuel-system performance due to manufacturing tolerances. The steady-state conditions at which the engine model was linearized are presented in Appendix B. The state-space form of the various linear engine models to be considered are given by the four matrices A, B, C, and D, for each of the 15 operating conditions described. The model format for the engine is as follows:

$$\begin{bmatrix}\dot{N}_H\\ \dot{N}_L\end{bmatrix}=\boldsymbol{A}\begin{bmatrix}N_H\\ N_L\end{bmatrix}+\boldsymbol{B}f$$

$$\begin{bmatrix}N_H\\ N_L\\ P_3\end{bmatrix}=\boldsymbol{C}\begin{bmatrix}N_H\\ N_L\end{bmatrix}+\boldsymbol{D}f$$

Manuscript received January 12, 1995; revised July 8, 1996. Recommended by Associate Editor, H. Geering. The first author was supported by a scholarship from Tenaga Nasional Malaysia Ltd.

The authors are with the Control Systems Centre, UMIST, Manchester M60 1QD, U.K.

Publisher Item Identifier S 1063-6536(97)01672-2.

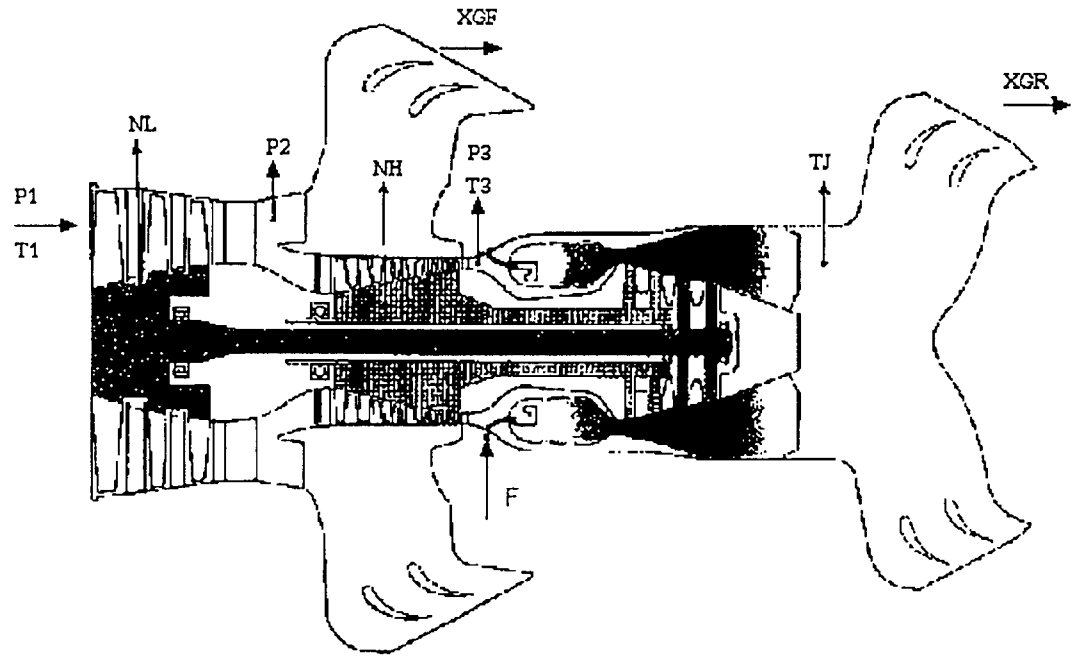

Fig. 1. The Pegasus aeroengine.

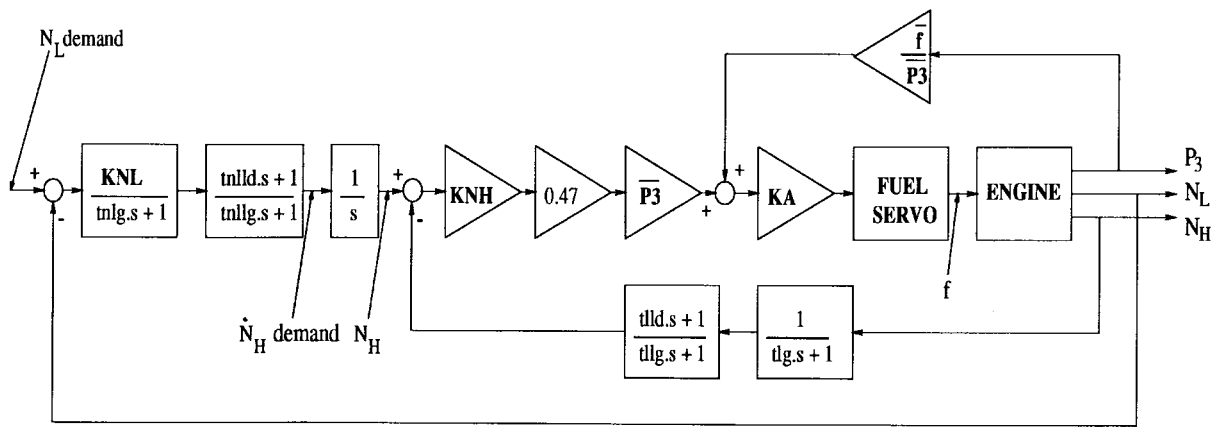

Fig. 2. Schematic diagram of the fan-speed control system.

where N_H is the speed of the high-pressure spool (%), N_L is the speed of the low-pressure spool or fan (%), P_3 is a pressure variable that influences the fuel-servo behavior (psi), and f is the fuel servo output (lb/h). The dimensions of the above matrices are as follows: $\boldsymbol{A}$ is 2 $\times$2, $\boldsymbol{B}$ is 2 $\times$1, $\boldsymbol{C}$ is 3 $\times$ 2, and $\boldsymbol{D}$ is 3 $\times$ 1.

Engine dynamical changes arise here from variations in its characteristics caused by the multiple fuelling conditions considered. The uncertainty to be expected in the fuel-system characteristics is presented in Figs. 10 and 11 (see Appendix A) in the form of Bode plots, showing maximum and minimum gain and phase variations from the nominal transfer-function behavior. The respective transfer functions concerned are as follows:

1) Nominal:

$$\frac{144.0}{s^2 + 16.8s + 144.0} \tag{1}$$

2) Maximum Gain Case:

$$\frac{299.48}{s^2 + 17.82s + 272.25} \tag{2}$$

3) Minimum Gain Case:

$$\frac{72.9}{s^2 + 12.6s + 81.0} \tag{3}$$

where the transfer-functions represent the linearized dynamical behavior of the fuel system, whose input signal is θ_{st} (in steps) (where θ_{st} represents the position of the fuel-servo stepper-motor denoted by $THST$ in Table III), and whose output is actual fuel-flow in lb/h.

The modulating effect of the compressor delivery pressure signal, P_3, on the fuel-system is shown in Fig. 2, and is taken into account in the system modeling to be described in the next section.

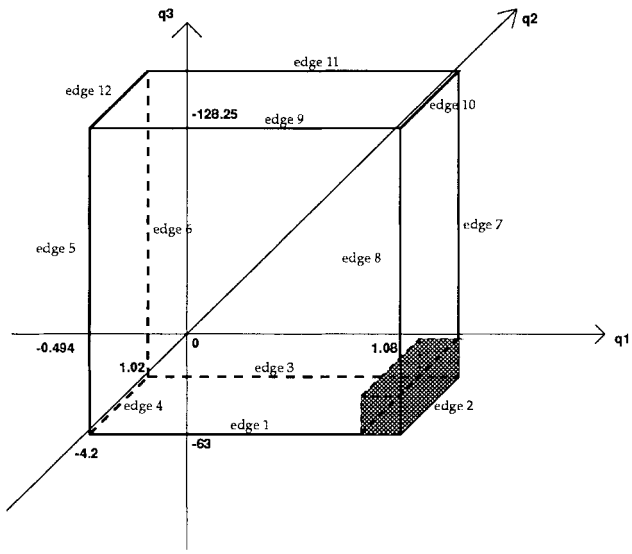

Fig. 3. Cuboid of the parameter space $\boldsymbol{q} \in Q$.

Based on these transfer-functions, the fuel-system transfer-function can be modeled as

$$G_f(s,\boldsymbol{q}) = \frac{144(1+q_1)}{s^2+(16.8+q_2)s+(144+q_3)} \tag{4}$$

where the interval parameters $q_i; i = 1,2,3;$ correspond to the effect of manufacturing tolerances on the coefficients of the locally linearized transfer-function model of the fuel system with

$$\begin{aligned} -0.4938 \le q_1 \le 1.0797 \\ -4.2 \le q_2 \le 1.02 \\ -63 \le q_3 \le 128.25. \end{aligned} \tag{5}$$

Here, $\boldsymbol{q} = [q_1 q_2 q_3]^T \in Q$ is the perturbation vector considered, and hence Q is a *cuboid* in the parameter space $\Re^3$. This notation is convenient for the subsequent mathematical manipulations of the uncertain parameters. The parameter box (hyperrectangle)[1] for the fuel-system is depicted in Fig. 3. Each point inside and on the edges of this cuboid corresponds to a possible value for the fuel-system perturbation vector and hence results in a different value for the fuel-system transfer-function. The objective now is to determine those values of the perturbation vector $\boldsymbol{q}$, for any point on the exposed edges[2] of this cuboid, which could give rise to undesirable closed-loop system performance.

B. State-Space Representation

A schematic diagram of the engine system considered is shown in Fig. 2. From this diagram, the state-space representations of the various subsystems concerned are determined as follows, where the subscripts $\boldsymbol{e}, \boldsymbol{f}, \boldsymbol{c}, \boldsymbol{ml}$, and $\boldsymbol{cl}$, applied to the subsystem components, refer to the basic engine, the fuel-servo, the forward-path controller, the minor-loop controller, and the overall closed-loop system, respectively.

[1] $Q = \{q\colon q_i^- \le q \le q_i^+, i = 1,2,\cdots,l\}$

[2] Exposed edges are the lines connecting two adjacent vertices.

For the engine

$$\begin{aligned} \dot{\boldsymbol{x}}_e &= \boldsymbol{A}_e \boldsymbol{x}_e + \boldsymbol{B}_e \boldsymbol{u}_e \\ \boldsymbol{y}_e &= \boldsymbol{C}_e \boldsymbol{x}_e + \boldsymbol{D}_e \boldsymbol{u}_e \end{aligned} \tag{6}$$

where $\boldsymbol{A}_e$ is $2\times 2, \boldsymbol{B}_e$ is $2\times 1, \boldsymbol{C}_e$ is 3×2 and $\boldsymbol{D}_e$ is 3×1.

The engine model given has the form

$$\begin{aligned} \begin{bmatrix} \dot{N}_H \\ \dot{N}_L \end{bmatrix} &= \boldsymbol{A}_e \begin{bmatrix} N_H \\ N_L \end{bmatrix} + \boldsymbol{B}_e \boldsymbol{u}_e \\ \begin{bmatrix} N_H \\ N_L \\ P_3 \end{bmatrix} &= \boldsymbol{C}_e \boldsymbol{x}_e + \begin{bmatrix} 0 \\ 0 \\ d \end{bmatrix} \boldsymbol{u}_e. \end{aligned} \tag{7}$$

For the fuel system

$$\begin{aligned} \dot{\boldsymbol{x}}_f &= \boldsymbol{A}_f \boldsymbol{x}_f + \boldsymbol{B}_f \boldsymbol{u}_f \\ \boldsymbol{y}_f &= \boldsymbol{C}_f \boldsymbol{x}_f \end{aligned} \tag{8}$$

where $\boldsymbol{A}_f$ is $2\times 2, \boldsymbol{B}_f$ is 2×1 and $\boldsymbol{C}_f$ is 1×2.

Since $\boldsymbol{u}_e = \boldsymbol{y}_f$, then

$$\begin{aligned} \dot{\boldsymbol{x}}_e &= \boldsymbol{A}_e \boldsymbol{x}_e + \boldsymbol{B}_e \boldsymbol{C}_f \boldsymbol{x}_f \\ \boldsymbol{y}_e &= \boldsymbol{y}_{cl} = \boldsymbol{C}_e \boldsymbol{x}_e + \boldsymbol{D}_e \boldsymbol{C}_f \boldsymbol{x}_f. \end{aligned} \tag{9}$$

For the N_L forward-path controller, we have

$$\begin{aligned} \dot{\boldsymbol{x}}_c &= \boldsymbol{A}_c \boldsymbol{x}_c + \boldsymbol{B}_c \boldsymbol{u}_c \\ \boldsymbol{y}_c &= \boldsymbol{C}_c \boldsymbol{x}_c \end{aligned} \tag{10}$$

where $\boldsymbol{A}_c$ is $3\times 3, \boldsymbol{B}_c$ is 3×1 and $\boldsymbol{C}_c$ is 1×3.

Since

$$\begin{aligned} \boldsymbol{u}_c &= \boldsymbol{N}_{\boldsymbol{L}_D} - \boldsymbol{N}_{\boldsymbol{L}} \\ &= \boldsymbol{N}_{\boldsymbol{L}_D} - \boldsymbol{m}_3 \boldsymbol{x}_e \end{aligned} \tag{11}$$

where the subscript D stands for demand, and $\boldsymbol{m}_3 = [0,\ 1]$, then

$$\dot{\boldsymbol{x}}_c = \boldsymbol{A}_c \boldsymbol{x}_c + \boldsymbol{B}_c \boldsymbol{m}_3 \boldsymbol{x}_e. \tag{12}$$

For the N_H minor-loop feedback controller, we have

$$\begin{aligned} \boldsymbol{u}_{ml} &= \boldsymbol{N}_{\boldsymbol{H}} \\ &= \boldsymbol{m}_2 \boldsymbol{x}_e \end{aligned} \tag{13}$$

where $\boldsymbol{m}_2 = [1,\ 0]$, and hence

$$\begin{aligned} \dot{\boldsymbol{x}}_{ml} &= \boldsymbol{A}_{ml} \boldsymbol{x}_{ml} + \boldsymbol{B}_{ml} \boldsymbol{m}_2 \boldsymbol{x}_e \\ \boldsymbol{y}_{ml} &= \boldsymbol{C}_{ml} \boldsymbol{x}_{ml}. \end{aligned} \tag{14}$$

Since

$$\boldsymbol{u}_f = \boldsymbol{K}_g[\boldsymbol{y}_c - \boldsymbol{y}_{ml}] + \frac{\overline{\boldsymbol{f}}}{\overline{\boldsymbol{P}}_{\boldsymbol{3}}} \boldsymbol{m}_1 \boldsymbol{y}_e \tag{15}$$

where $\boldsymbol{m}_1 = [0,\ 0,\ 1], \boldsymbol{K}_g = \boldsymbol{KNH}(0.47)\overline{\boldsymbol{P}}_3, \boldsymbol{KA} = 1$, and the *bar* over the variables $\boldsymbol{f}$ and $\boldsymbol{P}_3$ implies that nominal values for the particular operating condition are used, we get

$$\begin{aligned} \dot{\boldsymbol{x}}_f = {} & \boldsymbol{A}_f \boldsymbol{x}_f + \boldsymbol{K}_g \boldsymbol{B}_f \boldsymbol{C}_c \boldsymbol{x}_c - \boldsymbol{K}_g \boldsymbol{B}_f \boldsymbol{C}_{ml} \boldsymbol{x}_{ml} \\ & + \frac{\overline{\boldsymbol{f}}}{\overline{\boldsymbol{P}}_3} \boldsymbol{B}_f \boldsymbol{m}_1 \boldsymbol{C}_e \boldsymbol{x}_e + \frac{\overline{\boldsymbol{f}}}{\overline{\boldsymbol{P}}_3} \boldsymbol{B}_f \boldsymbol{m}_1 \boldsymbol{D}_e \boldsymbol{C}_f \boldsymbol{x}_f. \end{aligned} \tag{16}$$

The resulting closed-loop system state-space matrices $\boldsymbol{A}_{cl}, \boldsymbol{B}_{cl}, \boldsymbol{C}_{cl}$ and $\boldsymbol{D}_{cl}$, are then as shown below. These have

been derived symbolically, as it is then a simple matter of substituting for the symbols with their actual values, as provided in Appendix B, to consider any particular operating condition of the closed-loop system. The uncertainty in the fuel-servo system, represented by the vector $\boldsymbol{q}$, can then easily be introduced into the fuel-system model of (8) by using the controllable canonical form for $\boldsymbol{A}_f, \boldsymbol{B}_f, \boldsymbol{C}_f$ and $\boldsymbol{D}_f$ and we have the equations shown at the bottom of the page.

The presence of uncertain parameters in the closed-loop system state-space description manifests itself in the coefficients of the system characteristic polynomial $p(s, \boldsymbol{q})$, as shown in Appendix C. Hence, there are 15 such characteristic polynomials; one for each operating condition (or power level). Inspection of $p(s, \boldsymbol{q})$ shows that this has an affine-linear perturbation structure; i.e., each coefficient of this polynomial depends affine-linearly on the elements of the perturbation vector $\boldsymbol{q}$ [4]. This allows us to utilize the celebrated *Edge theorem* [7], which states that if a polynomial family is a polytope,[3] then the root locations of the polynomials contained on the exposed edges of the polytope completely determine the domain of the roots of every member of the polynomial family. Thus, in subsequent analysis of the system root-space, it is only necessary to examine the behavior of these limited sets in the s-plane.

III. Root Space Analysis

Since there are 15 operating conditions that can be analyzed, only one is chosen now for the sake of brevity, which is the 9000 lb/h operating level, where the scalar gains KNL and KNH, shown in Fig. 2 as part of a given control scheme, are 2.5 and 4.8, respectively. Applying the robust root locus (RRL) tool, as described by Barmish and Tempo [4], with the *Edge theorem* [7] at a constant gain, the system was found to be unstable for some $\boldsymbol{q} \in Q$ (Fig. 4), since there are distinct possibilities that some of the resultant poles will lie in the right-half plane. Here, we shall concern ourselves primarily with the analysis of poles near the imaginary axis, since these are the locations where the poles have the greatest potential to move to unstable regions in the complex plane.

[3] A polytope of polynomials is the higher dimensional generalization of a convex polygon in two dimensions.

Under closer scrutiny, this plot shows that each of the nine poles of the system have their own closed-boundaries. These are the regions around the nominal values corresponding to variations induced by the vector $\boldsymbol{q}$ for values inside and on the edges of the parameter space cuboid Q (see Fig. 3). The shaded box, shown in this figure, does not indicate the exact points of instability; it simply indicates the region in the parameter space to be avoided. Due to the uniqueness of the mapping between the uncertainty parameter space and the complex plane [2], the cuboid appears to be mapped around the nominal poles. There are nine of these *mapped-cuboids* around each of the nine nominal poles. It is easier to comprehend this by imagining that the plot is a distorted two-dimensional representation of a three-dimensional object. Nevertheless, we note that it is possible that some overlapping of these pole regions will result in nonseparability of these in the complex plane. The extreme boundaries of the mapping of the exposed-edges due to two or more adjacent poles appear, at certain operating conditions, to merge and produce a larger closed-region.

In Fig. 4, there are regions shown around the nominal poles at $-30 \pm 7.31\boldsymbol{I}$ (N_H minor-loop controller), $-5.59 \pm 8.06\boldsymbol{I}$ (fuel system), and $-2.73 \pm 2.31\boldsymbol{I}$ (engine). The region around the pole at -4.07 (N_L controller) appears to be mapped onto a line on the real axis. The same occurs for the double pole at -28.57 (N_L controller) except for the fact that, at this particular operating point, these poles are totally insensitive to variations in the perturbation vector $\boldsymbol{q}$, since they are in fact unobservable. These invariant real poles belong to the forward-path compensator. They are exactly cancelled-out by the same poles of the N_H minor-loop compensator at this operating condition, since the latter become zeros of the minor-loop subsystem with respect to the forward-path compensator.

Consider now the *mapped-cuboids* around the nominal poles $-2.73 \pm 2.31\boldsymbol{I}$ and $-5.59 \pm 8.06\boldsymbol{I}$, since these are the only regions where extreme perturbations could cause instability to the system. It can clearly be inferred from this plot that the *volume* at the bottom right of the cuboid (identified in Fig. 3) has to be avoided; ie the perturbation vector must not have values in this region in order to prevent the possibility of instability occuring. We are only interested, at this juncture,

$$\boldsymbol{A}_{cl} = \begin{bmatrix} \boldsymbol{A}_e & \boldsymbol{B}_e\boldsymbol{C}_f & 0 & 0 \\ \frac{\overline{\boldsymbol{f}}}{\overline{\boldsymbol{P}}_3}\boldsymbol{B}_f\boldsymbol{m}_1\boldsymbol{C}_e & \boldsymbol{A}_f + \frac{\overline{\boldsymbol{f}}}{\overline{\boldsymbol{P}}_3}\boldsymbol{B}_f\boldsymbol{m}_1\boldsymbol{D}_e\boldsymbol{C}_f & -\boldsymbol{K}_g\boldsymbol{B}_f\boldsymbol{C}_{ml} & \boldsymbol{K}_g\boldsymbol{B}_f\boldsymbol{C}_c \\ \boldsymbol{B}_{ml}\boldsymbol{m}_2 & 0 & \boldsymbol{A}_{ml} & 0 \\ -\boldsymbol{B}_c\boldsymbol{m}_3 & 0 & 0 & \boldsymbol{A}_c \end{bmatrix}$$

$$\boldsymbol{B}_{cl} = \begin{bmatrix} 0 \\ 0 \\ 0 \\ \boldsymbol{B}_c \end{bmatrix}$$

$$\boldsymbol{C}_{cl} = [\boldsymbol{C}_e \mid \boldsymbol{D}_e\boldsymbol{C}_f \mid 0 \mid 0]$$

$$\boldsymbol{D}_{cl} = \begin{bmatrix} 0 \\ 0 \\ 0 \end{bmatrix}$$

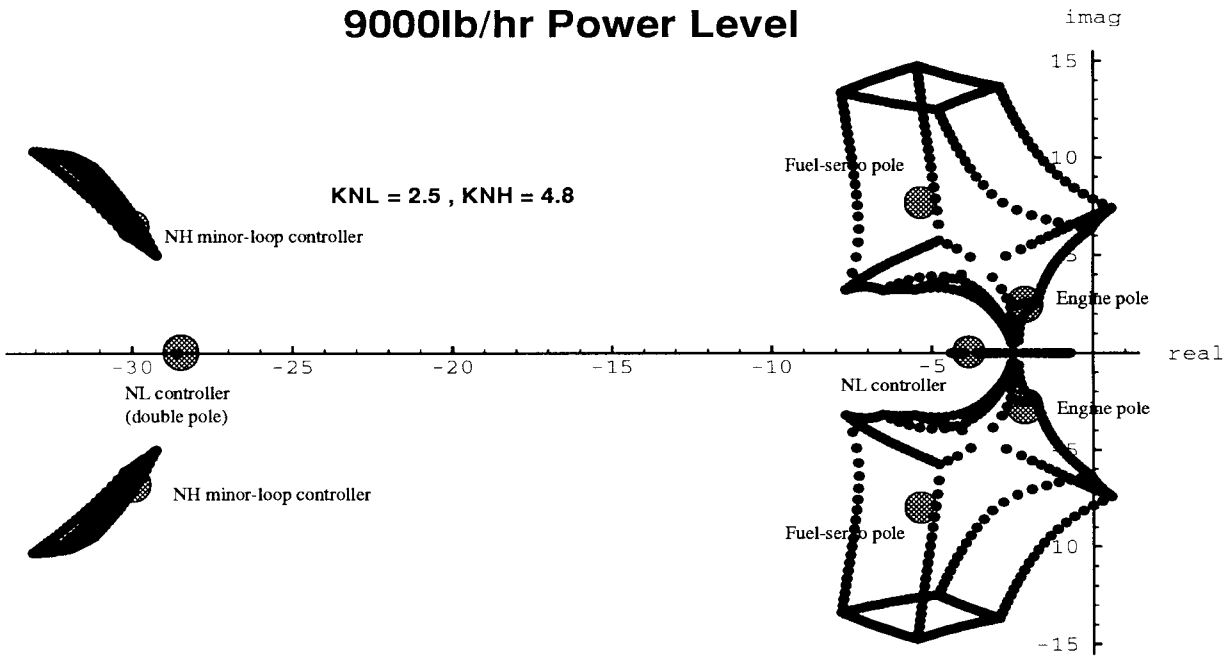

Fig. 4. Root space in the complex plane at 9000 lb/h.

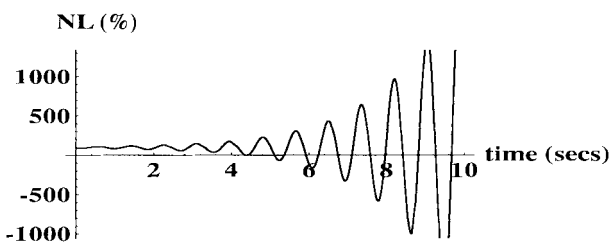

Fig. 5. Step applied at $(q_1^{\max}, q_2^{\min}, q_3^{\min})$.

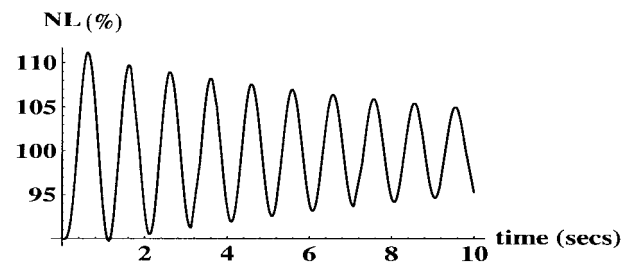

Fig. 6. Step applied at $(q_1^{\max}, q_2^{\max}, q_3^{\min})$.

in possible system instability due to parameter perturbation. Therefore, the region mentioned before must be avoided at all cost before any further design is attempted on the system.

The root-space analysis above has been repeated for various other fuel-consumption levels (namely 5000, 8000, 10 000, and 11 000 lb/h) with their respective inner and outer-loop controllers. For these other power levels, as we reduce the fuel-consumption rate, the pole-region mentioned before appears to move further to the left. Possible instability only occurs at the 8000 lb/h condition and above. At 5000 lb/h and below, the pole boundaries of the four poles of the two subsystems (engine and fuel-servo) are distinguishable, and it can be inferred that the poles of the engine approach instability along the real axis. In this case, the regions around the nominal poles of the fuel system are well within the second and third quadrants of the complex plane. This seems to suggest that as we move toward a higher fuel-consumption rate, the possible region of instability will become larger. However, it appears that the region of instability is smaller at the fuel-consumption rate of 10 000 lb/h than at 9000 lb/h and 11 000 lb/h. This is contradictory to the deduction just made, that a higher fuel-consumption rate will imply a larger instability region. This can, however, possibly be attributed to the fact that the controller dynamics are somehow not optimized for some of the operating levels. This is not to say that the system will immediately go unstable with the specified controller design parameter values, since the instability region occurs only for the small volume at the bottom right-hand edge of the parameter-space cuboid Q. It depends on whether or not the perturbation vector $\boldsymbol{q}$, arising from the manufacturing tolerances in the fuel-servo system, will assume certain values. The interested reader is encouraged to verify the above observations by creating the *root space plots* for the 5000 through 11 000 lb/h power levels, using the model data given in Appendix B.

Whilst the analysis given above could have been conducted using other methods, as there are only three uncertain parameters involved, the *Edge theorem* has shown its usefulness as one means of looking at a robustness problem. No single tool is a cure-all for all robustness problems and this theorem is one of a range tools which can be brought to bear. For example, since the dimension of the uncertainty is low, we could have generated 10 000 admissible triples (q_1, q_2, q_3) and for each such triple, the roots and the frequency responses could have been computed. This can easily be carried out using Matlab [1] with an extra program loop for the variation of the gain at this three-dimensional level, and there would have been no problem with excessive central processing unit (CPU) time.

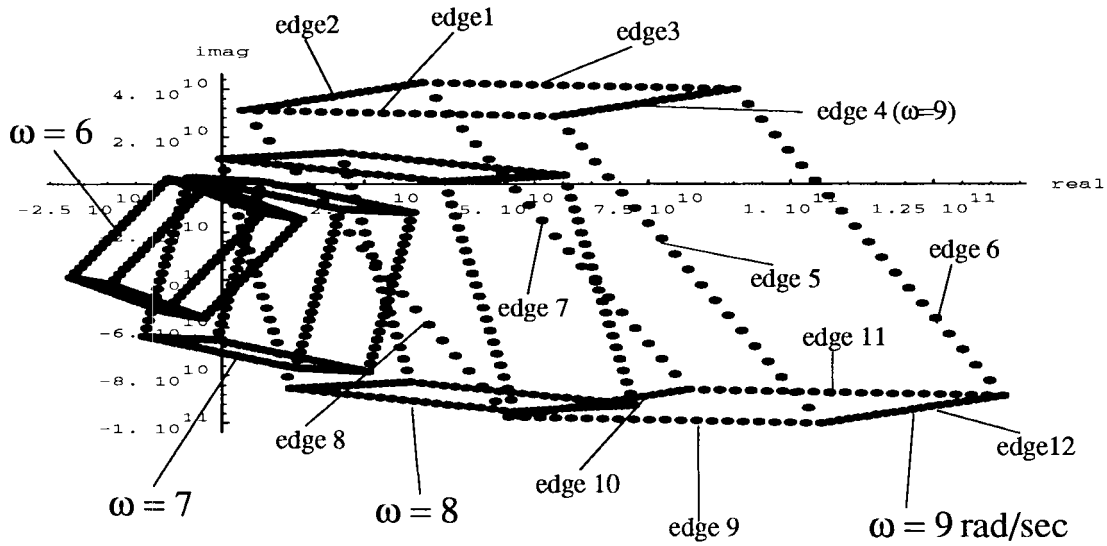

Fig. 7. Value sets for $\omega = 6, 7, 8$ and 9 rad/s.

IV. Step Responses

To further confirm that certain $\boldsymbol{q}$'s really do cause the system to go unstable, the vector $\boldsymbol{q}$ is set to values corresponding to the two vertices $\boldsymbol{v}_1 = (q_1^{\max}, q_2^{\min}, q_3^{\min})$ and $\boldsymbol{v}_2 = (q_1^{\max}, q_2^{\max}, q_3^{\min})$ at the 9000 lb/h operating point. A step input, resulting in a change in fuel-consumption of 1000 lb/h, is then applied to the low-pressure spool speed-reference input N_{L_D} at sea level static condition and the resulting time-response is reproduced for the closed-loop system state-space representation developed earlier, using the algebraic computing language Mathematica [12]. Since every power level has its own specified controller, this exercise is a rather crude approximation to reality, since it is assumed that the controller scheduling algorithm does not alter the controller parameters when this step is actually applied. The responses shown in Figs. 5–6 were obtained.

The response obtained for $\boldsymbol{q} = \boldsymbol{v}_1$ is clearly unstable. On the other hand, the response for $\boldsymbol{q} = \boldsymbol{v}_2$, while giving a rather oscillatory behavior, does depict a stable system; albeit one which takes a comparatively long time to settle down. Nevertheless, this oscillatory response obtained is wholly undesirable in most practical systems, hence it is to be avoided.

Repeating the same procedure on all of the power levels, we obtain instability at both vertices only for the 8000 lb/h operating point, thus proving the larger instability region. Our graphical inspection of the engine system with the RRL demonstrates that the offending region in the parameter space can be identified. However, determining the exact boundary of instability has not been attempted, since this would require the gridding of a great many $\boldsymbol{q}$ values.

V. Zero Exclusion Test

In this section, further checks are made (for the 9000 lb/h operating level) using the *zero exclusion theorem* [7] via the closed-loop characteristic polynomial (see Appendix C) of the overall system. Since, as in all other cases met before, it is not practical to check this condition individually for each and every $\omega \geq 0$, because this would involve a very large number of repetitions, a range of discrete ω values are chosen to perform this test ($\omega = 1, 2, 3, \cdots, 10$ rad/s). It will be further shown that this is sufficient to determine the robust frequency-domain stability characteristics of the system.

From an inspection of Fig. 7, it can be seen that the origin is contained in the closed-region bounded by the points generated by the characteristic polynomial when $\omega = 7$ rad/s. Hence, this confirms that the system is not robustly stable. It is relatively simple to check the stability here, since the ω values chosen will make the examination obvious by graphical inspection. Caution must be exercised, however, for general structures of characteristic polynomials, as there may just be cases when a *singular frequency* [2] occurs which requires special attention in the frequency domain methods.

VI. Robust Enhancement

So far, we have considered the closed-loop stability of the engine system in terms of the fuel-servo system uncertainty, using the given values of forward-path and minor-loop controller parameters. Clearly, the instability problem observed could be cured by tightening up the manufacturing tolerances for the fuel-servo system (with ensuing cost increases). Alternatively, it may be possible to avoid this instability by retuning certain controller parameters.

A. Gain Adjustment

There is one variable in each of the engine control loops that can be easily adjusted to give a more robust system, as considered in some earlier work on this problem by Kontogiannis [8]. For this particular investigation, we will concentrate on the 10 000 lb/h operating point, as this roughly gives a similar root space, to that considered earlier, for the exposed edges of Q.

First, we consider fixing KNL at its design value, and varying KNH. It was found that when KNH is restricted to lie between three and four (nominal value 4.8), the system provides the best root-space with respect to avoiding possible

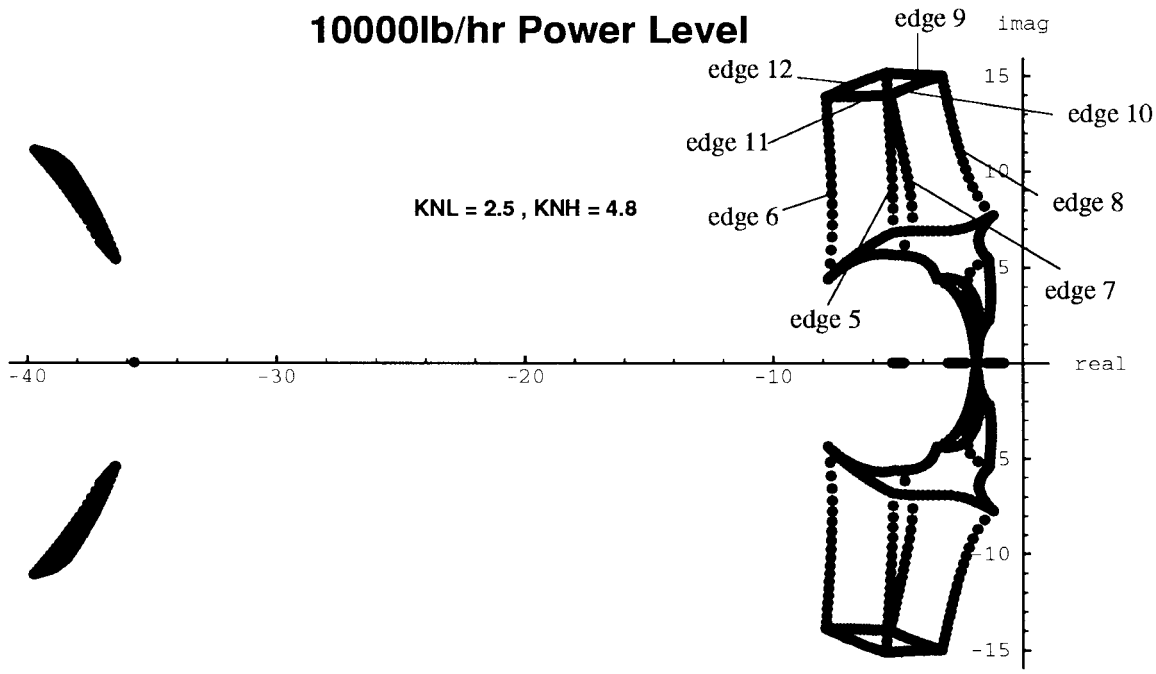

Fig. 8. Root-space in the complex plane with -20% change in dynamics.

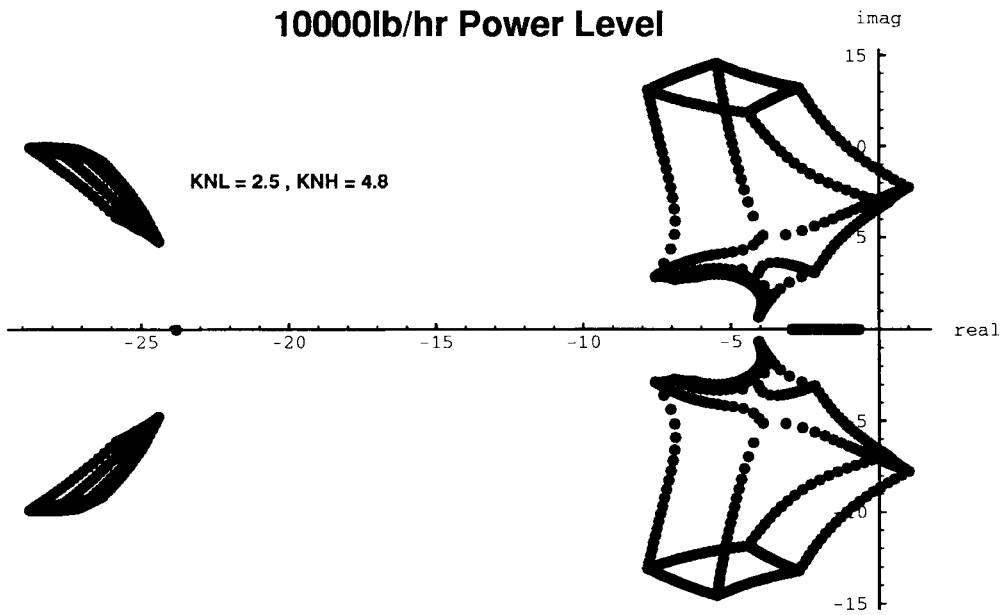

Fig. 9. Root-space in the complex plane with $+20\%$change in dynamics.

instabilities. As higher values of KNH are applied, the poles of the fuel and engine subsystems are more separable, but the region due to the former moves further into the right-hand side of the complex plane. If, however, we set KNH to have lower values than three, possible instabilities due to the engine poles might occur, as these approach the origin along the real axis.

Next KNH is fixed at its design value, and KNL is adjusted to lie between 0.1 and five (nominal value 2.5). As KNL is reduced, the poles concerned shift away from the imaginary axis. Nevertheless, care must again be exercised as the extreme regions of the engine poles can again approach the origin along the real axis, if low values of KNL are used. Thus, we conclude this section by suggesting that a best combination of the forward-path and minor-loop controller gains might be obtained by using the nominal value of KNH (4.8) and lower values for KNL.

B. Dynamics Adjustment

We next considered varying the dynamics of the controllers, while keeping the gains constant at their respective nominal design values. Here, for simplicity, the forward-path controller

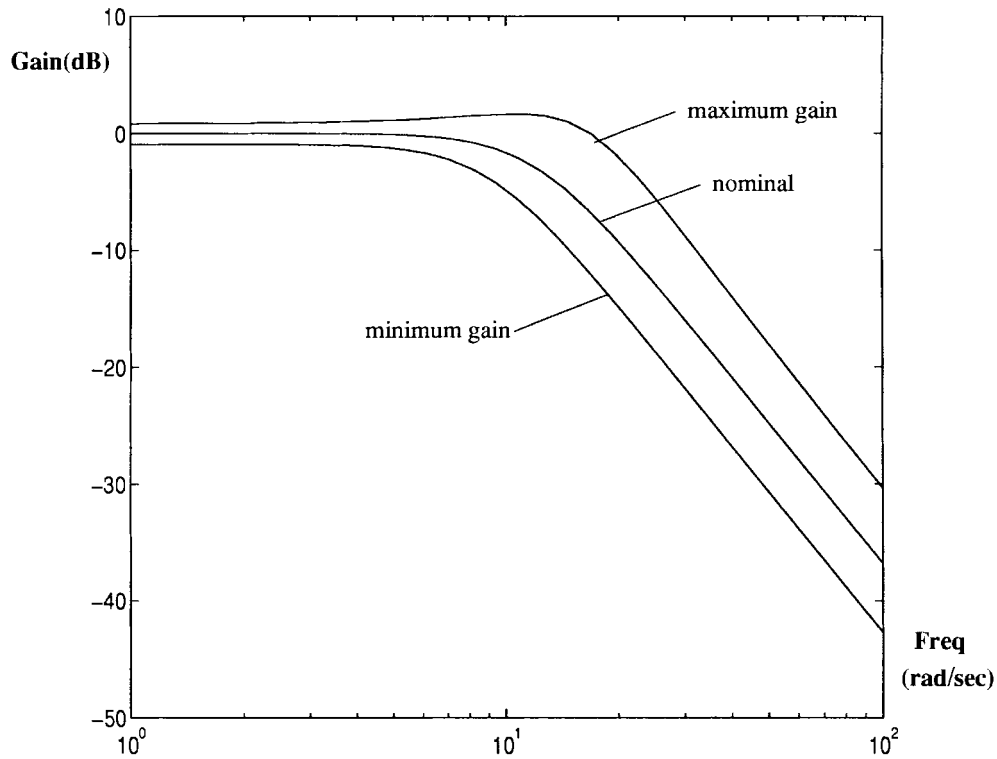

Fig. 10. Fuel system gain limits.

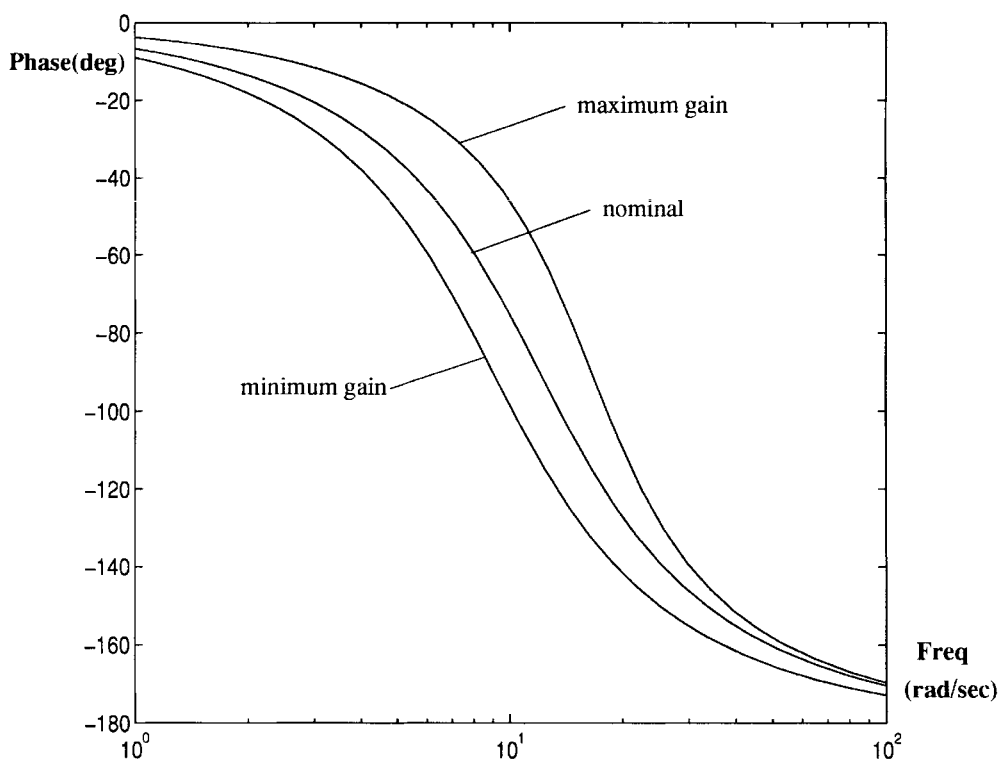

Fig. 11. Fuel system phase limits.

$(tnlld, tnllg$ and $tnlg)$ and minor-loop controller $(tllg$ and $tlg)$ dynamics are simultaneously varied, while retaining the structure of the compensators concerned, to see if we can improve the robustness of the system.

Here, it can be seen, as shown in Figs. 8 and 9, that a simple 20% decrease of the selected compensator dynamics will improve the stability robustness of the system. Conversely, a 20% increase will give a larger region of possible

instability. We conclude from these simple experiments that an improvement in the robust stability of the system can be observed, once the robust root-locus of the system is obtained. This will facilitate any subsequent analysis, since the dynamics of the system can be readily adjusted and the corresponding root-space generated.

It was not felt at this point appropriate to consider any further investigations into the determination of the best controller parameters, since those already determined by the subcontractor concerned were no doubt arrived at by taking other aspects of the engine behavior, such as surge, fuel-rate, and temperature limits, into account.

VII. Conclusions and Suggestions

We have seen in this paper how the closed-loop poles of a control system may be highly sensitive to the coefficients of the corresponding characteristic polynomial. A control system design which looks good when determined using only nominal model values, may have poles which are badly smeared over a large region in the complex plane, when known uncertainties are explicitly taken into account. Hence, having the RRL available as an analysis tool, has provided the opportunity to check whether or not this phenomenon is occuring. Subsequently, it has been shown that by retuning the loop gain and/or the dynamics of the controllers concerned, a more desirable distribution of closed-loop poles can be obtained. Said in another way, the RRL and zero exclusion theorem can be readily used for robustness enhancement.

With regard to the investigation being conducted on a relatively simple model, it is worth noting that this is a real problem provided by industry, in this case Rolls-Royce. The formulation of the parameter settings in the problem may seem to be a rather crude approximation to reality, but the variations are physically attainable due to manufacturing tolerances, with only their limits quantified.

Further work could be done on this problem by optimizing the design of the compensator dynamic terms with respect to parameter uncertainties. It may also be possible to study the robustness of the system with respect to transitions between operating points (i.e., the controller scheduling) using a development of the approaches used. A full nonlinear model of the engine system has been provided and is now being used in further studies of this system.

Appendix A
Gain and Phase Plots

See Figs. 10 and 11.

Appendix B
Steady-State Conditions

See Tables I–V.

TABLE I
Forward-Path Controller Parameter Values

NLdemand (%)	**tnlld** (sec)	**tnllg** (sec)	**tnlg** (sec)	**KNL** (%/sec/%)
10	0.5	0.05	0.05	0.5
20	0.5	0.05	0.05	0.5
30	0.5	0.05	0.05	0.5
40	0.47	0.047	0.047	0.5
50	0.44	0.044	0.044	0.5
60	0.41	0.041	0.041	0.5
70	0.38	0.038	0.038	0.75
80	0.35	0.035	0.035	1.5
90	0.35	0.035	0.035	2.5
100	0.35	0.035	0.035	2.5
110	0.35	0.035	0.035	2.5

TABLE II
MINOR-LOOP CONTROLLER PARAMETER VALUES

NH (%)	**tlld** (sec)	**tllg** (sec)	**tlg** (sec)	**KNH** (steps/%)
50	0.2	0.035	0.035	10.4
55	0.2	0.035	0.035	10.24
60	0.2	0.035	0.035	9.4
65	0.2	0.035	0.035	8.56
70	0.2	0.035	0.035	7.6
75	0.2	0.035	0.035	6.0
80	0.2	0.035	0.035	5.6
85	0.2	0.035	0.035	5.2
90	0.2	0.035	0.035	4.8
95	0.2	0.035	0.035	4.8
100	0.2	0.035	0.035	4.8

TABLE III
LINEARIZATION POINTS AT SEA LEVEL STATIC CONDITIONS

Fuel (lb/hr)	**P3** (psi)	**NH** (%)	**NL** (%)	**THST** (steps)
12470	165.5	95.6	100.0	160
11000	153.6	93.6	95.9	152.6
10000	144.8	92.2	93.0	146.7
9000	135.9	90.7	89.9	140
8000	126.4	89.0	86.6	135.5
7000	115.5	87.0	82.7	129.1
6000	105.0	85.0	78.5	122.6
5000	92.6	81.9	73.1	116.2
4000	79.5	78.4	66.6	108.1
3000	64.7	74.1	57.4	99
2000	47.5	66.0	43.3	91.4
1000	26.3	46.5	23.0	82.5

TABLE IV
LINEARIZATION AT THREE FLIGHT CONDITIONS

Mach	**Alt** (feet)	**Fuel** (lb/hr)	**P3** (psi)	**NH** (%)	**NL** (%)
0.6	50000	2100	27.3	100.4	91.2
1.2	50000	3500	46.4	99.9	94.9
0.8	0	17000	227.7	100.25	98.6

TABLE V
ENGINE A, B, C, AND D MATRICES

Fuel(lb/hr)	**A**		**B**	**C**		**D**
12470	-5.1035	0	0.0062	1	0	0
	2.2402	-3.7779	0.0068	0	1	0
				0.1381	1.6777	0.0038
11000	-4.5301	0	0.0063	1	0	0
	2.3365	-3.8822	0.0074	0	1	0
				0.1366	1.5640	0.0038
10000	-4.5811	0	0.0064	1	0	0
	2.3943	-3.7608	0.0078	0	1	0
				0.1419	1.6136	0.0031
9000	-4.6311	0	0.0065	1	0	0
	2.4425	-3.7724	0.0083	0	1	0
				0.1350	1.4938	0.0038
8000	-3.3600	0	0.0066	1	0	0
	2.5453	-3.9952	0.0089	0	1	0
				0.1396	1.6319	0.0038
7000	-3.4313	0	0.0067	1	0	0
	2.6317	-3.6503	0.0095	0	1	0
				0.1598	1.5862	0.0038
6000	-2.7523	0	0.0068	1	0	0
	2.6842	-3.6267	0.0102	0	1	0
				0.1461	1.4301	0.0038
5000	-2.3701	0	0.0072	1	0	0
	2.6854	-3.3454	0.0108	0	1	0
				0.1659	1.4717	0.0034
4000	-2.0200	0	0.0080	1	0	0
	2.5757	-2.9147	0.0115	0	1	0
				0.1862	1.4740	0.0038
3000	-1.2721	0	0.0087	1	0	0
	2.2307	-2.2600	0.0114	0	1	0
				0.1663	0.9270	0.0038
2000	-0.9452	0	0.0095	1	0	0
	1.5190	-1.4990	0.0098	0	1	0
				0.1333	0.9443	0.0032
1000	-0.3296	0	0.0097	1	0	0
	0.3227	-0.5603	0.0034	0	1	0
				-0.0171	0.8950	0.7629e-03
2100	-0.7527	0	0.0069	1	0	0
	0.3219	-0.4670	0.0067	0	1	0
				0.0220	0.1781	0.0036
3500	-1.4062	0	0.0065	1	0	0
	0.6144	-1.0663	0.0070	0	1	0
				0.0359	0.4803	0.0036
17000	-6.5632	0	0.0060	1	0	0
	3.4131	-5.2991	0.0072	0	1	0
				0.2106	2.3323	0.0031

APPENDIX C
CHARACTERISTIC POLYNOMIALS AT 9000 lb/h

Listed below is the characteristic polynomial $p(s, \boldsymbol{q})$ for the 9000 lb/h operating level.

```
3.994879664394982 10  + 3.994879664394982 10  q1 +
                    9                        9
     3.72765015639889 10  s + 2.051193962373067 10  q1 s +
                    7                          9  2
     1.16420569029571 10  q3 s + 1.560371218491067 10  s  +
                     8     2                     7     2
     3.236807953577719 10  q1 s  + 1.16420569029571 10  q2 s  +
                     6     2                     8  3
     7.229887966413998 10  q3 s  + 3.62898971986298 10  s  +
                    6     3                      6     3
     8.61682756177078 10  q1 s  + 7.229887966413998 10  q2 s  +
                    6     3                      7  4
     1.53595812281816 10  q3 s  + 5.037602691530442 10  s  -
                     6     4                      6     4
     2.306912084091617 10  q1 s  + 1.53595812281816 10  q2 s  +
                      4                        6  5
     136451.0734002566 q3 s  + 4.493102350422103 10  s  -
                      5                        5
     181353.2600455093 q1 s  + 136451.0734002566 q2 s  +
                      5                        6
     5875.829545313471 q3 s  + 248259.5885513053 s  -
                     6                         6
     4572.668067360456 q1 s  + 5875.829545313471 q2 s  +
                      6                        7
     122.6892142857143 q3 s  + 8044.76993471745 s  -
                      7                          7       7
     36.23841059602649 q1 s  + 122.6892142857143 q2 s  + q3 s  +
                     8       8    9
     139.4892142857143 s  + q2 s  + s
```

REFERENCES

[1] *User's Guide to Matlab: High-Performance Numeric Computation and Visualization Software*, 1992.

[2] J. Ackermann, *Robust Control Systems with Uncertain Physical Parameters*. Berlin: Springer-Verlag, 1993.

[3] B. Barmish, "A generalization of Kharitonov's four polynomial concept for robust stability problems with linearly dependent coefficient perturbations," *IEEE Trans. Automat. Contr.*, vol. 34, pp. 157–165, 1989.

[4] B. Barmish and R. Tempo, "The robust root locus," *Automatica*, vol. 26, no. 2, pp. 283–292, 1990.

[5] B. A. Francis, *A Course in H^∞ Control*, number 88 in Lecture Notes in Control and Information Sciences Edition. Berlin: Springler-Verlag, 1987.

[6] M. Fu, "Computing the frequency response of linear systems with parametric pertubations," *Syst. Contr. Lett.*, vol. 15, pp. 45–52, 1990.

[7] A. Bartlett, C. Hollot, and Huang-Lin, "Root locations of an entire polytope of polynomials: It suffices to check the edges," *Mat. Contr., Signals, Syst.*, vol. 1, pp. 61–71, 1988.

[8] E. Kontogiannis, "Robustness analysis tools and pole placement," Master's thesis, Univ. Manchester Inst. Sci. Technol., U.K., 1993.

[9] A. W. Olbrot, M. Fu, and M. P. Polis, "Introduction to the parametric approach to robust stability," *IEEE Contr. Syst. Mag.*, vol. 8, pp. 7–11, 1989.

[10] J. M. Maciejowski, *Multivariable Feedback Design*. Reading, MA: Addison-Wesley, 1989.

[11] A. G. Shutler, "A case study problem for the advanced controls technology club," Rolls-Royce Ltd., Tech. Rep., 1991.

[12] S. Wolfram, *Mathematica: A System for Doing Mathematics by Computer*, 2nd ed. Reading, MA: Addison-Wesley, 1993.

Aznan E. Ariffin received the B.Eng. degree in electrical engineering from Imperial College, London, in 1993 and M.Sc. degree in control and information technology from University of Manchester Institute of Science and Technology (UMIST), U.K., in 1994.

He is on a study leave from Tenaga Nasional Limited of Malaysia and currently pursuing the Ph.D. degree in UMIST. His research interests are continuous and switching gain scheduling control and linear parameter varying systems.

Neil Munro (S'71–M'76–SM'90–F'97) received the Ph.D. degree from the University of Manchester Institute of Science and Technology, (UMIST), U.K., in control engineering in 1969, and the D.Sc. degree from Manchester University in 1982.

He is Professor of Applied Control Engineering at UMIST, and was Head of the Control Systems Centre from 1987 to 1996. His research interests include the development and application of multivariable control theory, and the related CAD tools, with his current research focusing on the use of symbolic algebra for developing improved CAD tools and the extension of the Kharitonov-based approach on robust control to multivariable systems. Application areas include aerospace and process control. He has published more than 150 technical articles, coauthored one textbook, and been editor/coeditor for three other textbooks.

Dr. Munro is currently the U.K. National Consultant to the EPSRC for the Control and Instrumentation Area, and is a Fellow of the IEE.